Journal of Non-Crystalline Solids 356 (2010) 2059–2065

Contents lists available at ScienceDirect

Journal of Non-Crystalline Solids

journal homepage: www.elsevier.com/ locate/ jnoncrysol

Solid-state synthesis and characterization of new cadmium and rare-earth metal molybdato-tungstates $Cd_{0.25}RE_{0.50}(MoO_4)_{0.25}(WO_4)_{0.75}$ (RE = Pr, Nd, Sm–Dy)

E. Tomaszewicz [a,*], G. Dąbrowska [a], S.M. Kaczmarek [b], H. Fuks [b]

[a] West Pomeranian University of Technology, Department of Inorganic and Analytical Chemistry, Al. Piastów 42, 71-065 Szczecin, Poland
[b] West Pomeranian University of Technology, Institute of Physics, Al.Piastów 17, 70-310, Szczecin, Poland

ARTICLE INFO

Article history:
Received 12 May 2010
Received in revised form 18 May 2010
Available online 14 June 2010

Keywords:
Cadmium and rare-earth double molybdato-tungstates;
WLEDs

ABSTRACT

New cadmium and rare-earth double molybdato-tungstates $Cd_{0.25}RE_{0.50}(MoO_4)_{0.25}(WO_4)_{0.75}$ (RE = Pr, Nd, Sm–Dy) were prepared by the solid-state reaction technique from $CdMoO_4$ and adequate $RE_2(WO_4)_3$. The obtained compounds crystallized in the scheelite-type structure and showed solubility in $CdMoO_4$ forming $Cd_xGd_{2-2x}(MoO_4)_x(WO_4)_{3-3x}$ solid solutions for $0.50<x<1.00$. All the obtained phases were characterized by XRD, DTA-TG, IR and EPR methods. The EPR measurements of gadolinium containing samples confirmed that Gd^{3+} ions were located at octahedral positions. With the increasing gadolinium content the exchange and dipole–dipole interactions led to a totally antiferromagnetic type of interaction in the Gd^{3+} chains network.

1. Introduction

White light-emitting diodes (WLEDs), called next-generation solid-state lighting, have attracted much attention in recent years because of their wide applications as well as their advantages over conventional light sources. High stability, low power consumption, safety and friendliness to the environment are some of the advantages of WLEDs. The great availability of white light-emitting diodes is the reason why they have found such exciting applications as: white light source to replace traditional incandescent and florescent lamps, backlights for portable electronics, architecture and medical lighting. Host candidates for luminescent applications are doped and undoped double rare-earth molybdates, tungstates or molybdato-tungstates such as: $Gd_2Mo_3O_9:Eu^{3+}$ [1]; $Gd_{2-x}Eu_x(MoO_4)_3$ [2]; $Gd_{0.8-x}Y_xEu_{1.2}(MoO_4)_3$ [2]; $Gd_{0.2}Y_{0.6-x}Eu_{1.2}Sm_x(MoO_4)_3$ [2]; $LiY_{1-x}Eu_x(MoO_4)_2$ [3]; $Sr_9R_{2-x}Eu_xW_4O_{24}$ (R = Gd and Y) [4]; $NaM(WO_4)_{2-x}(MoO_4)_x:Eu^{3+}$ (M = Y, Gd) [5], $LiEu(WO_4)_{2-x}(MoO_4)_x$ [6] and $Gd_{2-y}Eu_y(WO_4)_{3-x}(MoO_4)_x$ [7].

It is well known that rare-earth metals can form a family of tungstates with the general formula $RE_2(WO_4)_3$ [8,9]. These tungstates adopt various structure types as a function of temperature and ionic radius of RE^{3+} ions. For RE = La–Dy, the $RE_2(WO_4)_3$ compounds crystallize in the monoclinic system, in the $C2/c$ space group [9,10]. Additionally, rare-earth tungstates, for the RE^{3+} cation ranging from Gd to Dy in size, show polymorphism. The high-temperature polymorphic modifications of $RE_2(WO_4)_3$ (RE = Gd–Dy) crystallize in the orthorhombic system [10]. The structure of low-temperature monoclinic polymorphs of $RE_2(WO_4)_3$ can be described as a scheelite-type structure ($CaWO_4$, S.G. $I4_1/a$) with one-third of the ordered vacancies in Ca^{2+} sites [9,10]. The RE^{3+} ions are surrounded by oxygen ions in a nearly regular eight-fold coordination [9]. Two distinct kinds of highly distorted WO_4 tetrahedra are observed in the structure of $RE_2(WO_4)_3$ [9]. According to other authors [10], there are slightly deformed WO_4 tetrahedra and strongly deformed trigonal bipyramids WO_5. Negative thermal expansion has been observed in some tungstates of general formula $RE_2(WO_4)_3$ [11–13].

In the present paper, new cadmium and rare-earth metal molybdato-tungstates $Cd_{0.25}RE_{0.50}(MoO_4)_{0.25}(WO_4)_{0.75}$ (RE = Pr, Nd, Sm–Dy) were synthesized by the solid-state reaction route using $RE_2(WO_4)_3$ and $CdMoO_4$. The obtained compounds as well as $Cd_xGd_{2-2x}(MoO_4)_x(WO_4)_{3-3x}$ solid solutions were characterized by XRD, DTA-TG, IR and EPR methods.

2. Experimental

2.1. Sample preparation

Cadmium molybdate ($CdMoO_4$) and rare-earth metal tungstates ($RE_2(WO_4)_3$, RE = Pr, Nd, Sm–Dy) were used as the starting materials for the experiments. Rare-earth tungstates were obtained by the solid-state reaction between RE_2O_3 (RE = Nd, Sm–Gd, Dy), Pr_6O_{11} or Tb_7O_{12} (all oxides with the purity degree of 99.9%, Aldrich) and WO_3 (99.9%, Fluka). Stoichiometric mixtures of an adequate rare-earth metal oxide with WO_3 were homogenized in an agate mortar and

* Corresponding author.
E-mail address: tomela@zut.edu.pl (E. Tomaszewicz).

0022-3093/$ – see front matter © 2010 Elsevier B.V. All rights reserved.
doi:10.1016/j.jnoncrysol.2010.05.044

Table 1
Results of indexing $Cd_{0.25}RE_{0.50}(MoO_4)_{0.25}(WO_4)_{0.75}$ powder diffraction patterns.

No.	*RE* = Pr		*RE* = Nd		*RE* = Sm		*RE* = Eu		*RE* = Gd		*RE* = Tb		*RE* = Dy		$CaWO_4$		*h*	*k*	*l*
	d_{obs}/nm	I/I_0	d_{obs}/nm	I/I_0	d_{obs}/nm	I/I_0	d_{obs}/nm	I/I_0	d_{obs}/nm	I/I_0	d_{obs}/nm	I/I_0	d_{obs}/nm	I/I_0	d_{obs}/nm	I/I_0			
1	0.4814	16	0.4793	19	0.4775	18	0.4753	11	0.4740	15	0.4735	19	0.4728	16	0.4765	84	1	0	1
2	0.3143	100	0.3131	100	0.3119	98	0.3107	90	0.3096	83	0.3093	100	0.3088	95	0.3105	100	1	1	2
3	0.3118	90	0.3112	100	0.3098	100	0.3089	100	0.3078	100	0.3074	100	0.3072	100	0.3071	30	1	0	3
4	0.2890	56	0.2889	30	0.2877	35	0.2864	28	0.2856	34	0.2852	30	0.2847	28	0.2843	39	0	0	4
5	0.2646	32	0.2633	40	0.2624	40	0.2611	31	0.2605	39	0.2602	36	0.2600	35	0.2621	19	2	0	0
6	0.2319	5	0.2308	3	0.2299	3	0.2288	4	0.2282	3	0.2279	3	0.2271	2	0.2296	18	2	1	1
7	0.2288	5	0.2283	3	0.2275	3	0.2263	4	0.2257	3	0.2253	3	0.2252	2	0.2256	3	1	1	4
8	0.2017	2	0.2009	2	0.2004	2	0.1992	2	0.1987	2	0.1984	1	0.1983	1	0.1994	10	2	1	3
9	0.1952	70	0.1946	45	0.1939	48	0.1929	42	0.1924	50	0.1922	45	0.1920	42	0.1928	36	2	0	4
10	0.1872	15	0.1862	15	0.1856	10	0.1846	9	0.1840	14	0.1838	15	0.1837	14	0.1854	15	2	2	0
11	0.1713	72	0.1711	26	0.1705	28	0.1696	21	0.1691	29	0.1689	30	0.1687	27	0.1688	17	1	1	6
12	0.1609	25	0.1600	20	0.1594	20	0.1587	19	0.1582	20	0.1581	18	0.1579	16	0.1592	23	3	1	2
13	0.1604	31													0.1587	4	3	0	3
14	0.1572	12	0.1565	10	0.1559	10	0.1551	9	0.1547	10	0.1546	12	0.1544	12	0.1553	13	2	2	4
15	0.1446	4	0.1445	4	0.1439	4	0.1432	3	0.1428	3	0.1427	3	0.1424	3	0.1422	4	0	0	8
16	0.1323	3	0.1317	2	0.1312	2	0.1306	3	0.1302	2	0.1300	2	0.1299	1	0.1311	2	4	0	0
17	0.1268	16	0.1266	15	0.1262	14	0.1256	10	0.1252	12	0.1251	8	0.1249	11	0.1250	7	2	0	8
18	0.1263	12	0.1260	10	0.1255	10	0.1249	11	0.1246	10	0.1244	6	0.1243	8	0.1248	11	3	1	6
19	0.1221	4	0.1214	4	0.1209	4									0.1208	4	3	3	2
20	0.1203	4	0.1198	4	0.1194	4	0.1188	5	0.1185	4	0.1183	3	0.1182	2	0.1190	7	4	0	4
21			0.1178	3	0.1173	4	0.1168	4	0.1165	4	0.1163	3	0.1162	3	0.1172	4	4	2	0
22	0.1144	3	0.1141	3	0.1137	3	0.1131	4	0.1129	3	0.1127	2	0.1126	2	0.1128	3	2	2	8
23	0.1105	3	0.1104	2	0.1099	2	0.1093	3	0.1091	2	0.1090	2	0.1088	2	0.1087	3	1	1	10
24	0.1097	3	0.1094	2	0.1090	3									0.1084	5	3	2	7
25			0.1043	2	0.1039	2	0.1034	2	0.1032	2	0.1030	2	0.1029	2	0.1035	2	3	3	6
26	0.1022	3	0.1017	2	0.1013	3	0.1008	3							0.1012	3	5	1	2

annealed at the following temperatures: 1123 K (12 h), 1173 K (12 h), 1223 K (12 h) and 1273 K (3×12 h) with several intermediate grindings. For the synthesis of cadmium molybdate, an equimolar mixture of CdO with MoO_3 (both 99.9%, Fluka) was heated in 12 h periods, at selected temperatures, starting from 823 K. The final temperature of heating of the CdO/MoO_3 mixture was 1273 K. The $RE_2(WO_4)_3/CdMoO_4$ mixtures were prepared with a range of rare-earth metal tungstates from 0.50 mol% to 90.00 mol%. All the mixtures were heated in an atmosphere of static air, in 12 h cycles and at the following temperatures: 1273 K, 1298 K and 1323 K (3×). For *RE* = Sm–Dy, the $RE_2(WO_4)_3/CdMoO_4$ mixtures were additionally heated at 1333 K and 1348 K (3×). After each heating period, all the mixtures were furnace cooled to room temperature, weighted, ground and examined for their content by the XRD method.

2.2. Measurements

The powder X-ray diffraction (XRD) measurements of the samples were carried out using a HZG-4 diffractometer. The data were collected from 10° to 100° (2Θ), using the step size of 0.02° and the counting time of 10 s per step under 35 kV and 35 mA with CuKα radiation (λ = 0.15418 nm). The error determining the position of the diffraction lines was 0.02° (2Θ°). The reflections (2Θ°) were indexed using the POWDER and DICVOL programs [14–17].

The DTA-TG studies were performed using SDT 2960 TA Instruments thermoanalyzer with the air flow (110 mL min^{-1}) at the heating rate of 10 K min^{-1}, and an open corundum crucible was used as the container.

The IR spectra were recorded on a Specord M-80 spectrometer. The measurements were performed in the wave number range of 1500–300 cm^{-1} at a resolution of 4 cm^{-1}. The investigated samples were pressed in pellets with KBr in the weight ratio of 1:100.

The EPR measurements were performed with a conventional X-band Brücker ELEXSYS E500 CW spectrometer operating at 9.5 GHz with 100 kHz magnetic field modulation. The temperature dependence of the EPR spectra was registered in the liquid nitrogen–295 K temperature range using the Oxford flow cryostat to control it.

3. Results and discussion

3.1. Reactivity in the solid-state between $RE_2(WO_4)_3$ (RE = Pr, Nd, Sm–Dy) and $CdMoO_4$

The XRD analysis results of the samples obtained after the last heating cycle of the $RE_2(WO_4)_3/CdMoO_4$ mixtures showed that these compounds were not mutually inert. The XRD analysis performed for the samples the initial mixtures of which contained above 50.00 mol% of $RE_2(WO_4)_3$ showed that two solid phases occurred in the samples

Table 2
Crystallographic characteristics of $Cd_{0.25}RE_{0.50}(MoO_4)_{0.25}(WO_4)_{0.75}$.

Compound	*a*/nm	*c*/nm	*c*/*a*	*Z*	*V*/nm^3	d_{exp}/g cm^{-3}	d_{cal}/g cm^{-3}	Reference
$Cd_{0.25}$**Pr**$_{0.50}(MoO_4)_{0.25}(WO_4)_{0.75}$	0.52948(9)	1.1559(1)	2.1831	4	0.32406(8)	6.49	6.40	This work
$Cd_{0.25}$**Nd**$_{0.50}(MoO_4)_{0.25}(WO_4)_{0.75}$	0.52662(7)	1.1555(9)	2.1949	4	0.32048(7)	6.60	6.51	This work
$Cd_{0.25}$**Sm**$_{0.50}(MoO_4)_{0.25}(WO_4)_{0.75}$	0.52476(7)	1.1510(1)	2.1934	4	0.31696(6)	6.70	6.65	This work
$Cd_{0.25}$**Eu**$_{0.50}(MoO_4)_{0.25}(WO_4)_{0.75}$	0.52216(4)	1.1454(7)	2.1937	4	0.31231(7)	6.82	6.76	This work
$Cd_{0.25}$**Gd**$_{0.50}(MoO_4)_{0.25}(WO_4)_{0.75}$	0.52075(9)	1.1424(3)	2.1938	4	0.30981(7)	6.95	6.87	This work
$Cd_{0.25}$**Tb**$_{0.50}(MoO_4)_{0.25}(WO_4)_{0.75}$	0.52008(6)	1.1411(8)	2.1942	4	0.30867(7)	7.00	6.92	This work
$Cd_{0.25}$**Dy**$_{0.50}(MoO_4)_{0.25}(WO_4)_{0.75}$	0.51956(5)	1.1396(6)	2.1935	4	0.30764(9)	7.05	6.98	This work
$CaWO_4$	0.5156(1)	1.1196(1)	2.1715	4	0.29765(2)		6.078	[18]

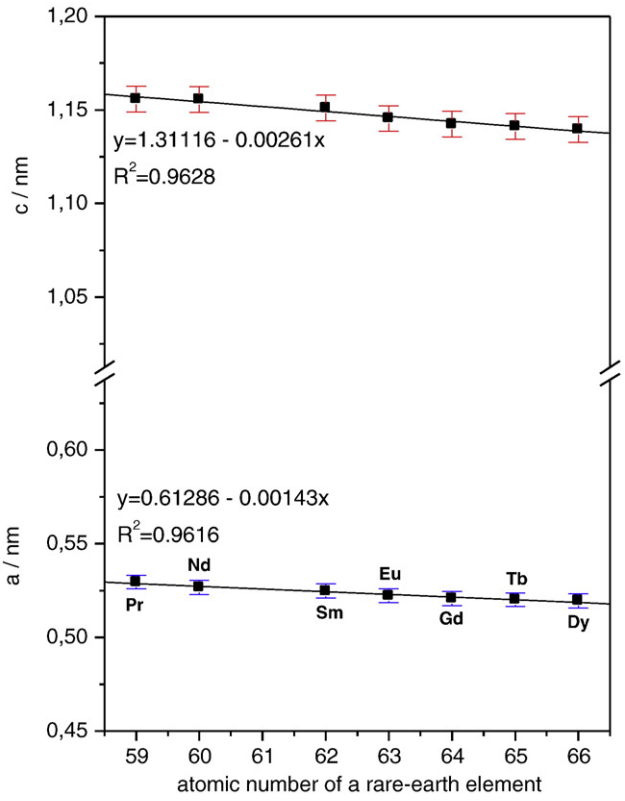

Fig. 1. Dependence of $Cd_{0.25}RE_{0.50}(MoO_4)_{0.25}(WO_4)_{0.75}$ lattice constants on rare-earth element's atomic number.

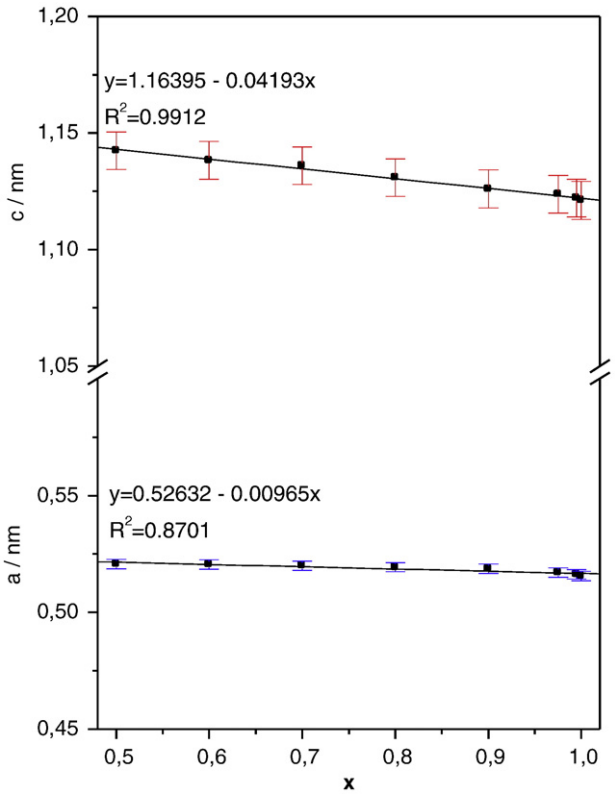

Fig. 2. Dependence of lattice constants of $Cd_xGd_{2-2x}(MoO_4)_x(WO_4)_{3-3x}$ solid solutions on $CdMoO_4$ content.

by treatment, viz. the compounds: $RE_2(WO_4)_3$ and new cadmium and rare-earth metal molybdato-tungstate $Cd_{0.25}RE_{0.50}(MoO_4)_{0.25}(WO_4)_{0.75}$. At the molar ratio 1:1 of the $RE_2(WO_4)_3/CdMoO_4$ mixtures, the prepared samples were pure single phases and their XRD powder patterns showed only diffraction lines characteristic for the scheelite-type structure. The new cadmium and rare-earth molybdato-tungstates are formed according to the following equation:

$$CdMoO_{4(s)} + RE_2(WO_4)_{3(s)} = 4Cd_{0.25}RE_{0.50}(MoO_4)_{0.25}(WO_4)_{0.75(s)} \quad (1)$$

The scheelite-type peaks were found also in the powder diffraction patterns of the samples obtained after annealing $RE_2(WO_4)_3/CdMoO_4$ mixtures comprising initially below 50.00 mol% $RE_2(WO_4)_3$. The positions of the scheelite-type diffraction lines were shifted towards higher 2Θ angles with the increasing cadmium molybdate content. Thus, $Cd_{0.25}RE_{0.50}(MoO_4)_{0.25}(WO_4)_{0.75}$ can form scheelite-type solid solutions with $CdMoO_4$. The formula of these solutions is $Cd_xRE_{2-2x}(MoO_4)_x(WO_4)_{3-3x}$ for $0.50<x<1.00$.

3.2. Characterization of $Cd_{0.25}RE_{0.50}(MoO_4)_{0.25}(WO_4)_{0.75}$ and the $Cd_xGd_{2-2x}(MoO_4)_x(WO_4)_{3-3x}$ solid solution by XRD and IR methods

Table 1 shows the results of indexing powder diffraction patterns of $Cd_{0.25}RE_{0.50}(MoO_4)_{0.25}(WO_4)_{0.75}$ as well as the values of interplanar

Table 3
Crystallographic characteristics of $CdMoO_4$, $Cd_{0.25}Gd_{0.50}(MoO_4)_{0.25}(WO_4)_{0.75}$ and $Cd_xGd_{2-2x}(MoO_4)_x(WO_4)_{3-3x}$ solid solutions for $x=0.60$; 0.70; 0.80; 0.90; 0.975 and 0.995.

Phase/composition of initial $RE_2(WO_4)_3/CdMoO_4$ mixture	a/nm	c/nm	c/a	V/nm^3	Reference
$Cd_{0.25}\mathbf{Gd}_{0.50}(MoO_4)_{0.25}(WO_4)_{0.75}$ ($Cd_{0.50}\mathbf{Gd}(MoO_4)_{0.50}(WO_4)_{1.50}$) (50.00 mol% $Gd_2(WO_4)_3$ + 50.00 mol% $CdMoO_4$)	0.52075(9)	1.1424(3)	2.1938	0.30981(7)	This work
$Cd_{0.60}\mathbf{Gd}_{0.80}(MoO_4)_{0.60}(WO_4)_{1.20}$ (40.00 mol% $Gd_2(WO_4)_3$ + 60.00 mol% $CdMoO_4$)	0.52057(8)	1.1382(6)	2.1865	0.30846(9)	This work
$Cd_{0.70}\mathbf{Gd}_{0.60}(MoO_4)_{0.70}(WO_4)_{0.90}$ (30.00 mol% $Gd_2(WO_4)_3$ + 70.00 mol% $CdMoO_4$)	0.51992(6)	1.1359(8)	2.1849	0.30708(2)	This work
$Cd_{0.80}\mathbf{Gd}_{0.40}(MoO_4)_{0.80}(WO_4)_{0.60}$ (20.00 mol% $Gd_2(WO_4)_3$ + 80.00 mol% $CdMoO_4$)	0.51932(3)	1.1308(6)	2.1776	0.30498(9)	This work
$Cd_{0.90}\mathbf{Gd}_{0.20}(MoO_4)_{0.90}(WO_4)_{0.30}$ (10.00 mol% $Gd_2(WO_4)_3$ 90.00 mol% $CdMoO_4$)	0.51865(6)	1.1259(7)	2.1709	0.30289(1)	This work
$Cd_{0.975}\mathbf{Gd}_{0.050}(MoO_4)_{0.975}(WO_4)_{0.075}$ (2.50 mol% $Gd_2(WO_4)_3$ 97.50 mol% $CdMoO_4$)	0.51700(7)	1.1236(7)	2.1734	0.30035(3)	This work
$Cd_{0.995}\mathbf{Gd}_{0.010}(MoO_4)_{0.995}(WO_4)_{0.015}$ (0.50 mol% $Gd_2(MoO_4)_3$ 99.50 mol% $CdMoO_4$)	0.51633(9)	1.1220(8)	2.1731	0.29915(2)	This work
$CdMoO_4$	0.51557(8)	1.1210(9)	2.1744	0.29800(9)	[19]

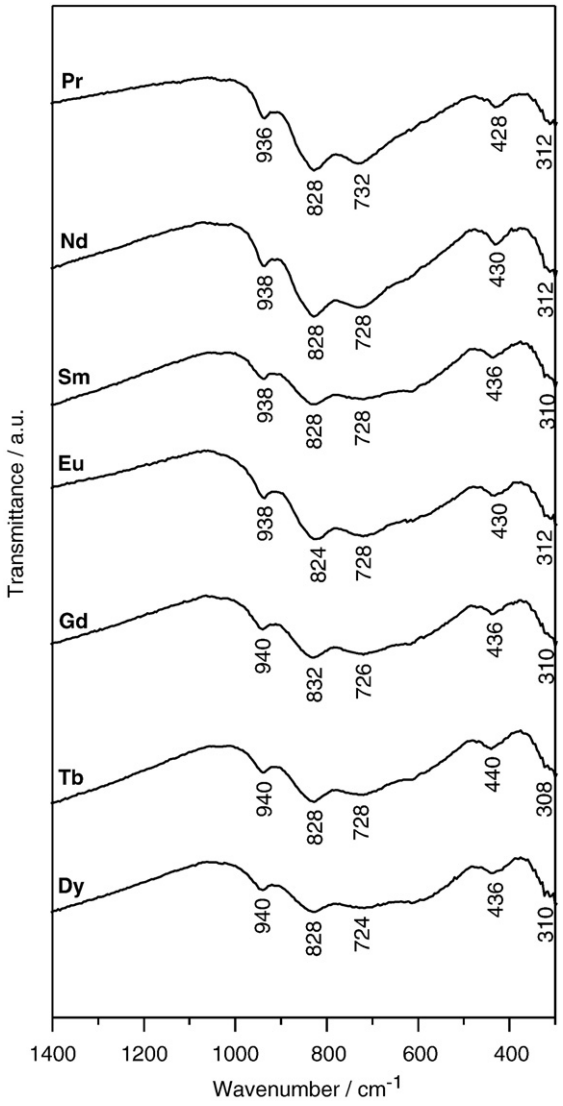

Fig. 3. IR spectra of $Cd_{0.25}RE_{0.50}(MoO_4)_{0.25}(WO_4)_{0.75}$ compounds.

distances for $CaWO_4$ (scheelite) [18]. The calculated lattice constants, the values of experimental (obtained by degassing of samples and hydrostatic weighing in CCl_4 as pycnometric liquid) and calculated density for $Cd_{0.25}RE_{0.50}(MoO_4)_{0.25}(WO_4)_{0.75}$ as well as for $CaWO_4$ are shown in Table 2. The data collected in Tables 1 and 2 confirm that $Cd_{0.25}RE_{0.50}(MoO_4)_{0.25}(WO_4)_{0.75}$ are isostructural and crystallize in the scheelite-type structure. The unit cell parameters of new cadmium and rare-earth molybdato-tungstates linearly decrease with an increase in the atomic number of a rare-earth element (Fig. 1). The calculated lattice constants for $Cd_{0.25}Gd_{0.50}(MoO_4)_{0.25}(WO_4)_{0.75}$, the $Cd_xGd_{2-2x}(MoO_4)_x(WO_4)_{3-3x}$ solid solutions ($x = 0.60$; 0.70; 0.80; 0.90; 0.975 and 0.995) as well as for $CdMoO_4$ are shown in Table 3. The unit cell parameters of the obtained solid solutions linearly decrease with the increasing $CdMoO_4$ content (Fig. 2).

Fig. 3 shows the IR spectra of $Cd_{0.25}RE_{0.50}(MoO_4)_{0.25}(WO_4)_{0.75}$. In the case of solid molybdates and tungstates with the scheelite-type structure (isolated MoO_4 and WO_4 tetrahedra) the stretching multiplets (ν_1 and ν_3) appear in the vibration frequencies of 908–675 cm^{-1} and 930–750 cm^{-1}, respectively [20–24]. In turn, the deformation modes (ν_2 and ν_4) appear in the 440–260 cm^{-1} (molybdates) and 420–250 cm^{-1} (tungstates) [20–24]. On the basis of the information contained in the literature on infrared spectroscopy of single and double molybdates and tungstates with the scheelite-type structure [20–25], the absorption bands observed in the IR spectra of $Cd_{0.25}RE_{0.50}(MoO_4)_{0.25}(WO_4)_{0.75}$ with the maxima at ~940 cm^{-1} can be attributed to the symmetric stretching modes of W–O bonds in WO_4 more than Mo–O bonds in MoO_4. However, the broad absorption bands centered around 830 and 728 cm^{-1} are due to the asymmetric stretching vibrations of W–O bonds in WO_4 tetrahedra. Analogously as for $Cd_{0.25}RE_{0.50}\square_{0.25}WO_4$ (the scheelite-type structure) [25], the absorption bands with the maxima located at around 436 and 310 cm^{-1} can be assigned to the symmetric and asymmetric deformation modes of W–O bonds in WO_4, respectively. The absorption bands connected with the stretching or deformation modes of Mo–O bonds in MoO_4 tetrahedra were not observed.

3.3. Thermal studies of $Cd_{0.25}RE_{0.50}(MoO_4)_{0.25}(WO_4)_{0.75}$ and the $Cd_xGd_{2-2x}(MoO_4)_x(WO_4)_{3-3x}$ solid solutions

Fig. 4 shows DTA curves of $Cd_{0.25}RE_{0.50}(MoO_4)_{0.25}(WO_4)_{0.75}$. Only one endothermic effect was observed on each DTA curve up to 1673 K. No mass losses were recorded on the TG curves (not presented here) up to the onset of each recorded effect on the DTA curves. The DTA studies and observations of the residues arising in crucibles after these examinations authorize the statement that effects with their onsets at: 1350 K (Pr); 1365 K (Nd); 1389 K (Sm); 1380 K (Eu); 1401 K (Gd); 1403 K (Tb) and 1399 K (Dy) are associated with congruent melting of these phases. To confirm this fact, separate samples of $Cd_{0.25}RE_{0.50}(MoO_4)_{0.25}(WO_4)_{0.75}$ were heated in a furnace for 4 h at a temperature selected from the range onset-minimum of each observed effect. After annealing, the mentioned samples were quickly quenched to 263 K. The diffraction patterns of the samples obtained in this way contained only peaks with very low intensities that could be attributed to $Cd_{0.25}RE_{0.50}(MoO_4)_{0.25}(WO_4)_{0.75}$. The DTA curves of the $Cd_xGd_{2-2x}(MoO_4)_x(WO_4)_{3-3x}$ solid solutions for four $CdMoO_4$ contents are shown in Fig. 5. The melting points of these solid solutions are higher that the melting point of $CdMoO_4$ (1408 K, [19]) and increase linearly with the increasing $CdMoO_4$ content (Fig. 6).

3.4. EPR studies of $Cd_{0.25}Gd_{0.50}(MoO_4)_{0.25}(WO_4)_{0.75}$ and $Cd_xGd_{2-2x}(MoO_4)_x(WO_4)_{3-3x}$ solid solutions

The electron paramagnetic resonance spectra of the $Cd_{0.25}Gd_{0.5}(MoO_4)_{0.25}(WO_4)_{0.75}$ sample observed at the range of 85–295 K show a wide and intense EPR line attributed to different Gd^{3+} paramagnetic centers. The EPR signal seems to be an envelope of an unresolved anisotropic fine structure of Gd^{3+} ions in powder. The shape of this line is almost of a pure Gaussian type (Fig. 7), which is a result of specific overlapping of the powder EPR spectrum, but additionally indicates possible dipole–dipole interactions between gadolinium ions. A similar shape of the resonance signal had been observed earlier for the $Cd_{0.25}Gd_{0.5}MoO_4$ compound [19]. However, contrary to the former report, the mixed molybdato-tungstate $Cd_{0.25}Gd_{0.5}(MoO_4)_{0.25}(WO_4)_{0.75}$ revealed complex behavior of the EPR line integral intensity, I. It is shown more clearly in Fig. 8, where the IT product as a function of temperature revealed a change in the inclination tendency of the dependence at c.a. 140 K. Negative inclination of the IT product below 140 K indicates a ferromagnetic type of interaction of Gd^{3+} ions, whereas above this temperature, when the inclination is positive, antiferromagnetic type interactions prevail. As the temperature increases, the EPR line changes the width and resonance position (Fig. 9), which confirms that the internal magnetic field and relaxation processes of Gd^{3+} paramagnetic centers are temperature dependent in this case, too.

Another part of the EPR investigation concerned $Cd_xGd_{2-2x}(MoO_4)_x(WO_4)_{3-3x}$ solid solutions with different content of gadolinium and cadmium ions. As could be expected, samples with small gadolinium

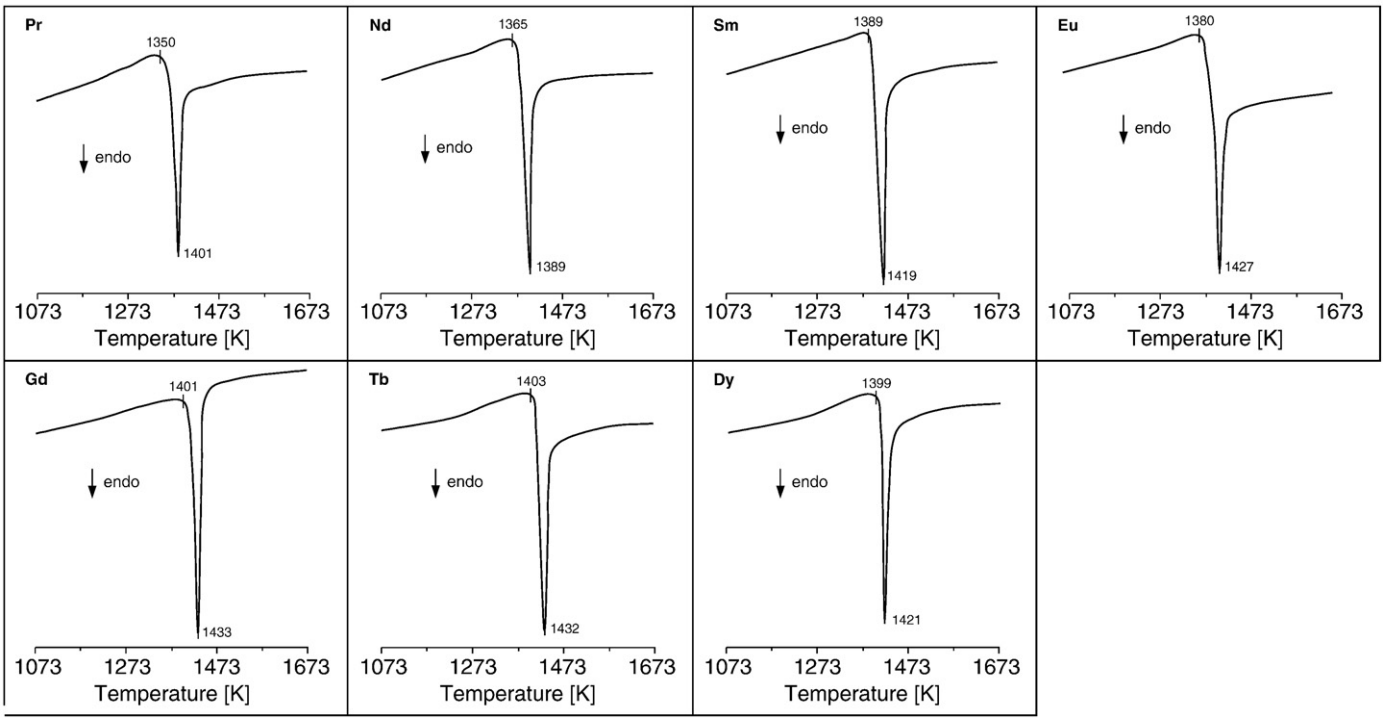

Fig. 4. DTA curves of $Cd_{0.25}RE_{0.50}(MoO_4)_{0.25}(WO_4)_{0.75}$ compounds.

content revealed resonance lines attributed to the isolated Gd^{3+} ions (Fig. 10). These ions were affected by a local crystal field giving a complex resonance signal with fine structure. As the concentration of Gd^{3+} ions increased, the EPR lines became wider due to more intense relaxation processes. With an increase in the Gd^{3+} ions content, the exchange interaction between Gd^{3+} ions became more significant, which was observed in the changes of θ parameter calculated according to the Curie–Weiss relation: $I = C/(T-\theta)$ (Table. 4).

Additionally, in the $Cd_{0.995}Gd_{0.01}(MoO_4)_{0.995}(WO_4)_{0.015}$ sample, where the gadolinium content was lower, the share of $CdMoO_4$ in the solid solution was more significant. As a result, a hyperfine structure of six narrow lines of pentavalent ^{95}Mo and ^{97}Mo isotopes ($S = 1/2$, $I = 5/2$) was observed in the EPR experiment (Fig. 11) for a wide temperature range.

A detailed analysis of the molybdenum signal allows estimating an average value of the A-hyperfine parameter as being equal to $A \sim 9.4$ mT. This value seems to be consistent with many reports concerning Mo^{5+} ions in different crystal matrices [26–28]. According to [26], where zirconia samples enriched with Mo^{5+} ions are analyzed, a less symmetric crystal environment leads to larger values of hyperfine A_i components. This behavior could be connected with a distortion of the MoO_4 tetrahedra, similarly as in the case of the analyzed sample.

4. Conclusions

New cadmium and rare-earth metal molybdato-tungstates with the formula $Cd_{0.25}RE_{0.50}(MoO_4)_{0.25}(WO_4)_{0.75}$ (RE = Pr, Nd, Sm–Dy) were synthesized by a conventional solid-state reaction between $CdMoO_4$ and $RE_2(WO_4)_3$. All the obtained phases crystallized in the scheelite-type structure and melted congruently in the temperature

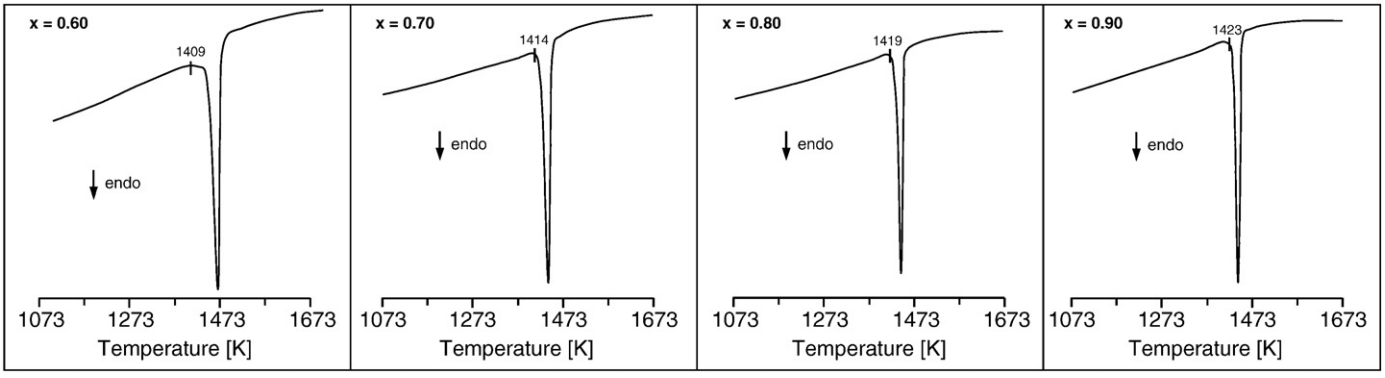

Fig. 5. DTA curves of some $Cd_xGd_{2-2x}(MoO_4)_x(WO_4)_{3-3x}$ solid solutions.

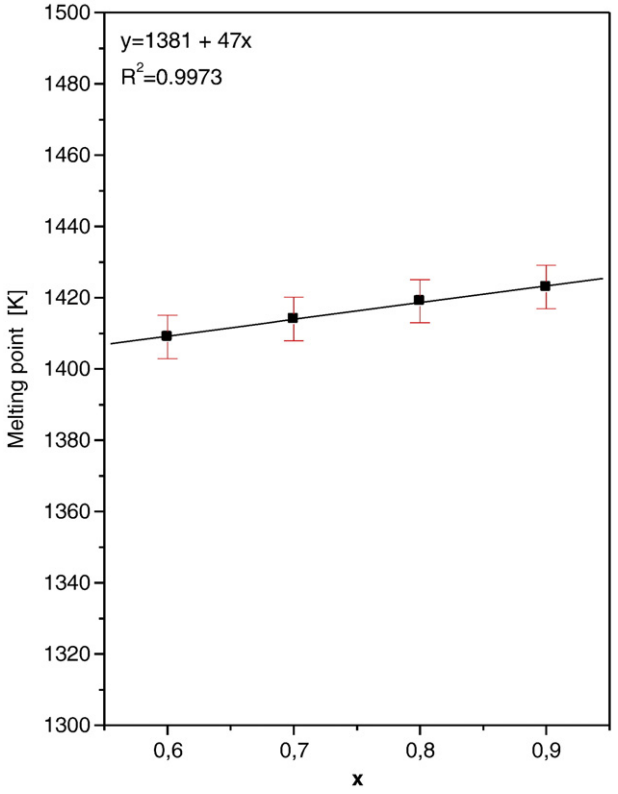

Fig. 6. Melting point composition dependence for some $Cd_xGd_{2-2x}(MoO_4)_x(WO_4)_{3-3x}$ solid solutions.

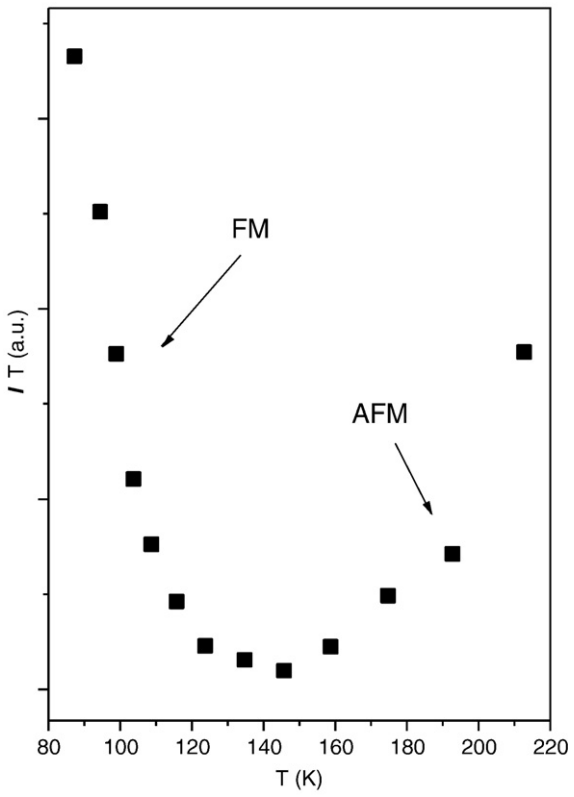

Fig. 8. *I*T product as a function of temperature for Gd^{3+} ions in $Cd_{0.25}Gd_{0.5}(MoO_4)_{0.25}(WO_4)_{0.75}$ compound.

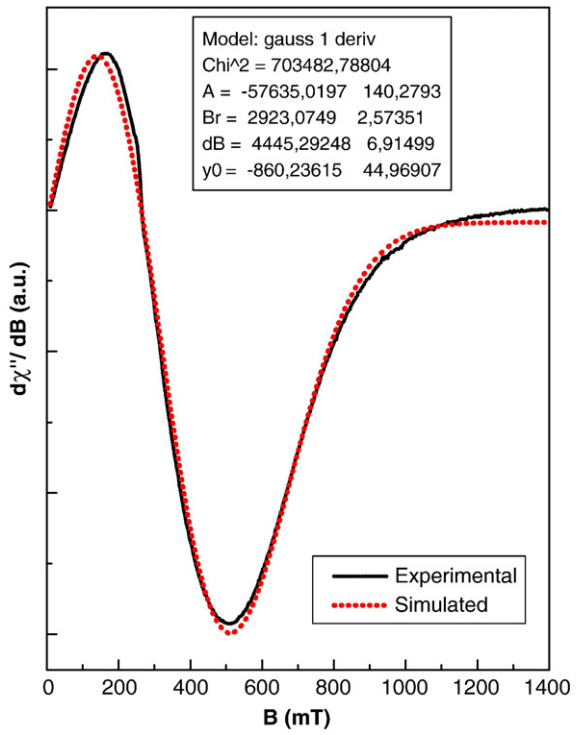

Fig. 7. EPR spectrum of $Cd_{0.25}Gd_{0.5}(MoO_4)_{0.25}(WO_4)_{0.75}$ sample at 88 K and its Gaussian fitting.

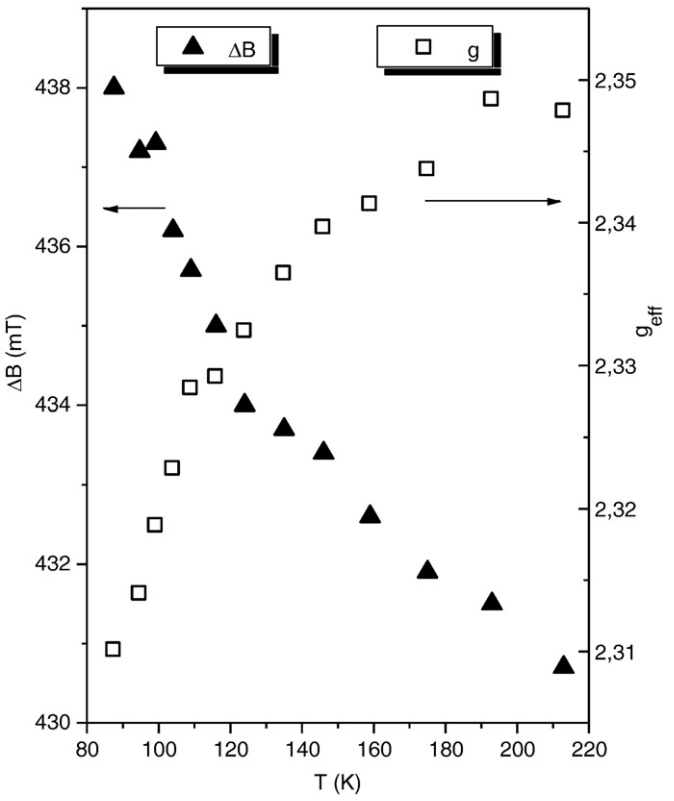

Fig. 9. Temperature dependence of EPR peak-to-peak line width (triangles) and effective g-spectroscopic parameter (squares) for Gd^{3+} ions in $Cd_{0.25}Gd_{0.5}(MoO_4)_{0.25}(WO_4)_{0.75}$.

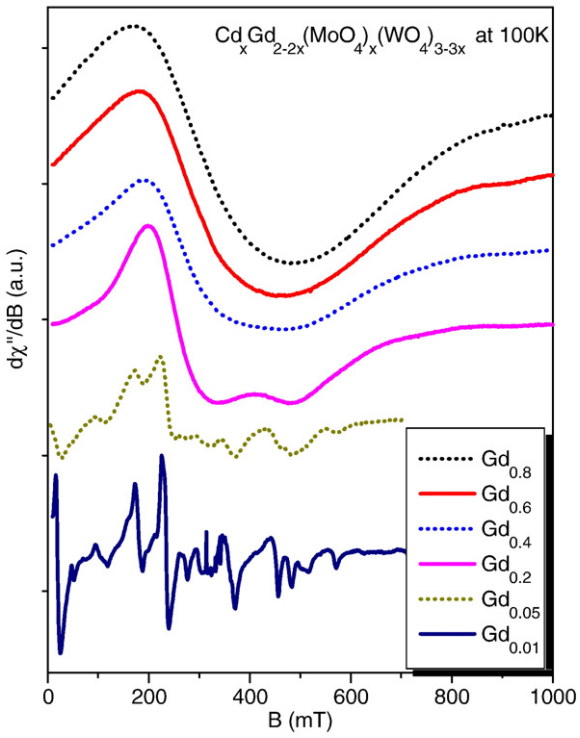

Fig. 10. EPR spectra of $Cd_xGd_{2-2x}(MoO_4)_x(WO_4)_{3-3x}$ solid solutions with different x content at 100 K.

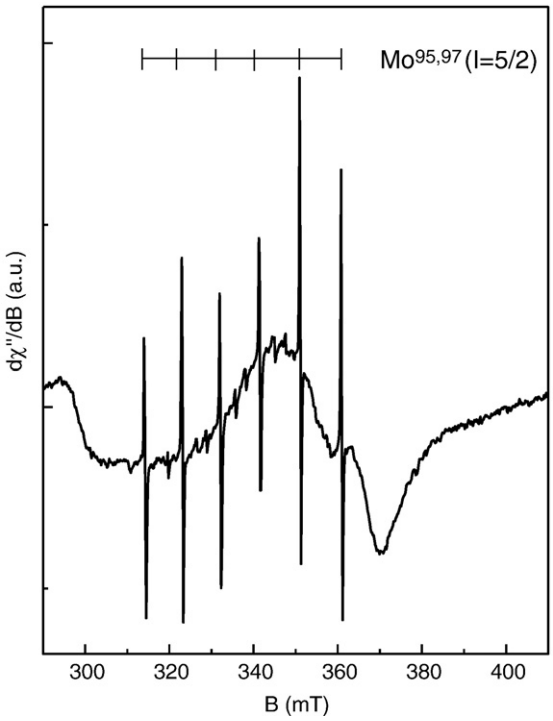

Fig. 11. Hyperfine structure of odd Mo^{5+} isotopes observed in gadolinium wide signal in $Cd_xGd_{2-2x}(MoO_4)_x(WO_4)_{3-3x}$ solid solutions with $x = 0.995$ at 220 K.

Table 4
Curie–Weiss relation temperature parameter for different concentrations of Gd^{3+} ions in $Cd_xGd_{2-2x}(MoO_4)_x(WO_4)_{3-3x}$ compound.

$2-2x$	0.01	0.05	0.2	0.4	0.6	0.8
θ	2.7	2.3	7.9	9.4	32.7	33.6

range of 1350–1403 K. $Cd_{0.25}RE_{0.50}(MoO_4)_{0.25}(WO_4)_{0.75}$ can form a solid solution with $CdMoO_4$ with the scheelite-type structure and the general formula $Cd_xRE_{2-2x}(MoO_4)_x(WO_4)_{3-3x}$ for $0.50<x<1.00$.

The EPR measurements of the gadolinium containing samples confirmed that Gd^{3+} ions were located at octahedral positions. With the increasing gadolinium content, an exchange and dipole–dipole interactions led to a total antiferromagnetic type of interaction in the Gd^{3+} chains network. The gadolinium content had influence on the local magnetic interaction and relaxation processes inside the analyzed compounds. It was the dipole–dipole magnetic interaction that dominated between the Gd^{3+} ions.

Acknowledgments

This scientific work is financed by the Polish budget resources allocated to science in the years 2009–2012 as research project N N209 336937.

References

[1] Z. Xiaoxia, W. Xiaojun, Ch. Baojiu, M. Qingyu, D. Weihua, R. Guozhong, Y. Yanmin, J. Alloys Compd. 433 (2007) 352.
[2] W. Xiao-Xiao, W. Jing, S. Jian-Xin, S. Qiang, G. Meng-Lian, Mat. Res. Bull. 42 (2007) 1669.
[3] A.V. Zaushitsyn, V.V. Mikhailin, A.Yu. Romanenko, E.G. Khaikina, O.M. Basovich, V.A. Morozov, B.I. Lazoryak, Inorg. Mat. 41 (2005) 766.
[4] Z. Qihua, H. Pei, P. Ming, L. Hongbin, G. Menglian, S. Qiang, Solid State Comm. 149 (2009) 880.
[5] S. Neeraj, N. Kijima, A.K. Cheetham, Chem. Phys. Lett. 387 (2004) 2.
[6] Ch. Chuang-Hung, W. Ming-Fang, L. Chi-Shen, Ch. Teng-Ming, J. Solid State Chem. 180 (2007) 619.
[7] W. Xiao-Xiao, X. Yu-Lun, S. Jian-Xin, S. Qiang, G. Meng-Lian, Mat. Sci. Eng. B 140 (2007) 69.
[8] K. Nassau, H.J. Levinstein, G.M. Loiacono, J. Phys. Chem. Solids 26 (1965) 1805.
[9] G.J. McCarthy, R.D. Fischer, J. Sanzgiri, J. Solid State Chem. 5 (1972) 200.
[10] A.A. Evdokimov, V.A. Ephremov, V.K. Trunov, I.A. Klejnman, B.F. Dzhyrinskij, Soedineniya Redkozemenykh Elementov. Molibdaty, volframaty, Nauka, Moskva, 1991 in Russian.
[11] S. Sumithra, A.M. Umarji, Solid State Sci. 6 (2004) 1313.
[12] S. Sumithra, A.M. Umarji, Solid State Sci. 8 (2006) 1453.
[13] P.M. Forster, A. Yokochi, A.W. Sleight, J. Solid State Chem. 140 (1998) 157.
[14] D. Taupin, J. Appl. Cryst. 1 (1968) 87.
[15] D. Taupin, J. Appl. Cryst. 6 (1973) 380.
[16] D. Louer, M. Louer, J. Appl. Cryst. 5 (1972) 271.
[17] A. Boultif, D. Louer, J. Appl. Cryst. 24 (1991) 987.
[18] F.N. Blanchard, Powder Diff. 4 (1989) 220.
[19] E. Tomaszewicz, S.M. Kaczmarek, H. Fuks, Mat. Chem. Phys. 122 (2010) 595.
[20] J. Hanuza, M. Mączka, J.H. van der Maas, J. Mol. Struct. 348 (1995) 349.
[21] G.M. Clark, W.P. Doyle, Spectrochim. Acta 22 (1966) 1441.
[22] R.G. Brown, J. Denning, A. Hallett, S.D. Ross, Spectrochim. Acta 26A (1970) 963.
[23] J. Hanuza, A. Benzar, A. Haznar, M. Maczka, A. Pietraszko, J.H. van der Maas, Vibr. Spectrosc. 12 (1996) 25.
[24] V.I. Tsaryuk, V.F. Zolin, Spectrochim. Acta A57 (2001) 355.
[25] E. Tomaszewicz, S.M. Kaczmarek, H. Fuks, J. Rare Earths 27 (2009) 569.
[26] D. Cordishi, M. Occhiuzzi, R. Dragone, J. Solid State Chem. 136 (1998) 263.
[27] B.B. Das, R. Ambika, Chem. Phys. Lett. 370 (2003) 670.
[28] U. Rogulis, Radiat. Meas. 29 (1998) 287.